SAND2020-11261C

Analysis of an Annular Coupled Patch Using CMA and CMT

John Borchardt and Tyler LaPointe
Sandia National Laboratories
Albuquerque, NM, USA
jjborch@sandia.gov

***Abstract*—This work analyses a low-profile, broadband monopole patch antenna (which we call the Annular Coupled Patch) using Characteristic Mode Analysis. The full structure is divided into two resonators: a cylindrical cavity and annular PIFA, which are electromagnetically coupled by the fringing fields about the annular ring of vias separating the two resonators. The analysis shows that Coupled Mode Theory accurately models the resonances of the full, coupled structure. The modal behavior is compared and contrasted with several other antennas that are also well-modeled by Coupled Mode Theory .**

Keywords—Annular patch, broadband patch, characteristic mode analysis, circular patch, coupled mode theory, monopole pattern, ring patch, wideband patch.

I. Introduction

The annular coupled patch (ACP) geometry is a low-profile structure that provides an omni-directional, monopole-like pattern with wide impedance bandwidth [1]. This paper uses Characteristic Mode Analysis (CMA) to analyze this geometry in a new way wherein the geometry is decomposed into two *coupled* resonators: a cylindrical cavity and annular PIFA. Fringing fields about the vias couple the two resonators, thereby providing wide impedance bandwidth (BW). Coupled Mode Theory (CMT) accurately describes the behavior of the coupled structure.

CMA [2] is a modal decomposition based on the method of moments (MoM) wherein a real, orthogonal basis J_n results from $[X]\,J_n = \lambda_n\,[R]\,J_n$ where $[Z] = [R] + j[X]$ is the MoM impedance matrix and λ_n is the eigenvalue [1]. Currents driven by a source can be expressed as a sum of modes: $J_{\text{total}} = \sum_n \alpha_n J_n$ where α_n are the modal weighting coefficients (MWCs) [2]. Thus, the driven admittance of a structure is the sum of all modal admittances. CMT describes the dynamics of a system of two coupled resonators as the superposition of two coupled modes, a lower-frequency in-phase and a higher-frequency anti-phase mode. The coupled mode frequencies $\omega_\pm = 2\pi f_\pm$ are related to the uncoupled mode frequencies $\omega_{1,2} = 2\pi f_{1,2}$ by [3]:

Sandia National Laboratories is a multimission laboratory managed and operated by National Technology & Engineering Solutions of Sandia, LLC, a wholly owned subsidiary of Honeywell International, Inc., for the U.S. Department of Energy's National Nuclear Security Administration under contract DE-NA0003525. This paper describes objective technical results and analysis. Any subjective views or opinions that might be expressed in the paper do not necessarily represent the views of the U.S. Department of Energy or the United States Government.

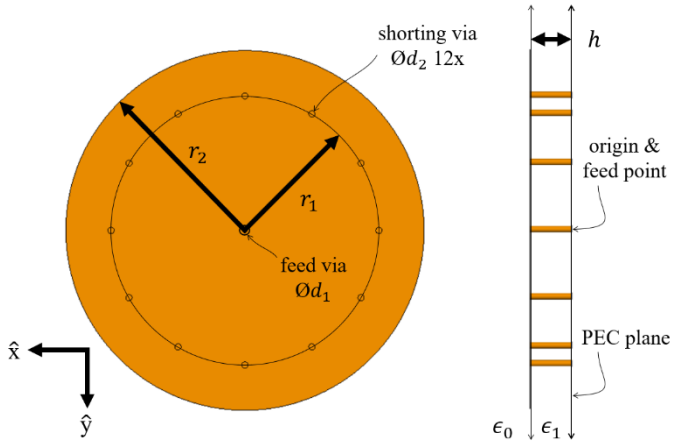

Fig. 1. Annular Coupled Patch geometry; (r_1, r_2, h, d_1, d_2) = (10.9, 15.4, 2.54, 0.38, 0.53) mm; $\epsilon_r = 3.55\epsilon_0$ There are N=12 shorting vias at radius r_1 equally distributed in angle.

$$\omega_\pm = \omega_0 \pm \sqrt{\left(\frac{\omega_2 - \omega_1}{2}\right)^2 + |K|^2} \qquad (1)$$

where $\omega_0 = (\omega_2 + \omega_1)/2$ and K is an un-normalized coupling coefficient.

II. Characteristic Mode Analysis

The geometry of Fig. 1 is solved in FEKO, a MoM code with CMA. A 1V gap source is located at the base of the center feed probe and is used for the driven solution excitation as well as for calculating modal admittances and modal weighting coefficients. The substrate is modeled as $\epsilon_r = 3.55\epsilon_0$; the dielectric and conductors are modeled as ideal.

The 6 dB return loss bandwidth is $4.51 - 6.49$ GHz, with band center at 5.5 GHz. There are several modes resonant near the impedance bandwidth, however, the modal weighting coefficients indicate that only two modes, modes 1 and 9, are strongly excited, as shown in Fig. 2. Eigenvalue crossing avoidance is evident; this phenomenon has been associated with coupled mode theory [4]. The modal charge distributions for these modes are shown in Fig. 3; in-phase and anti-phase relationships between the charge polarities with respect to their ground plane images on the patch outer edge and the center region are evident; such charge distributions are evidence of coupled mode phenomenon [5]-[8].

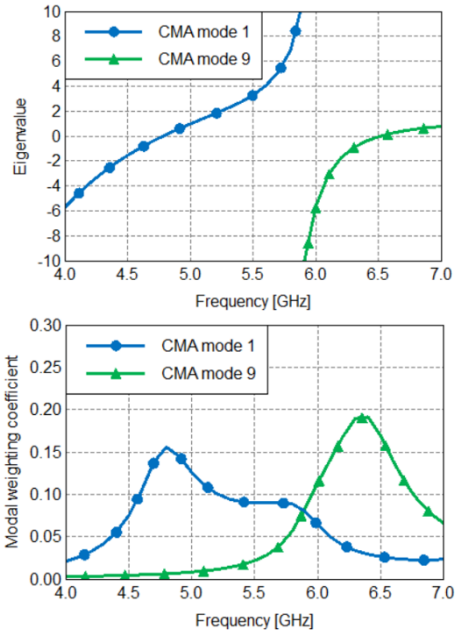

Fig. 2. CMA mode 1 and 9 eigenvalues and modal weighting coefficients.

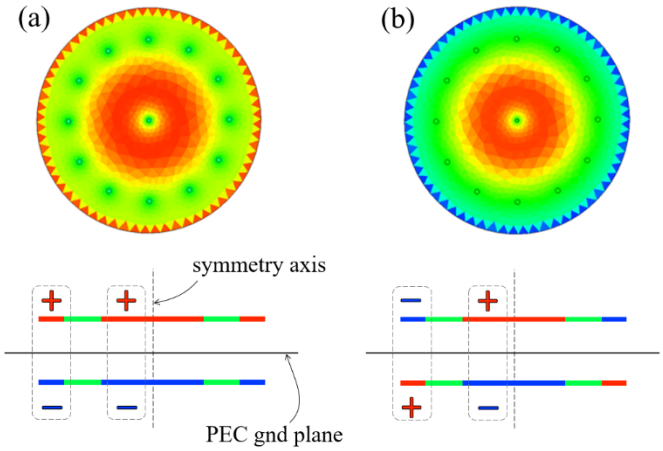

Fig. 3. Charge distributions for (a) mode 1 and (b) mode 9 near their respective resonances show in-phase and anti-phase relationships. Side views are shown at bottom.

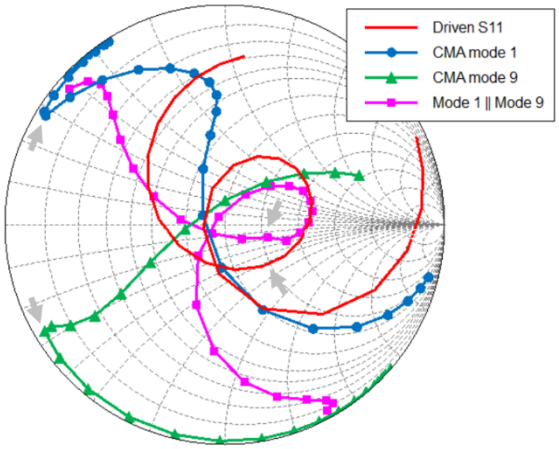

Fig. 5. The sum of mode 1 and 9 admittances replicates that of the driven problem. The grey arrows mark 5.9 GHz as discussed in Section V.

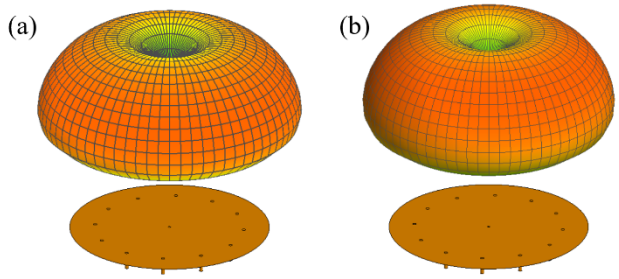

Fig. 4. $\hat{\theta}$-polarized radiation patterns for (a) mode 1 and (b) mode 9 near their respective resonances; both patterns are monopole-like with negligible cross-polarization.

Fig. 2 shows that modes 1 and 9 are resonant ($\lambda_n = 0$) at $f_- = 4.79$ GHz and $f_+ = 6.50$ GHz with modal Q's of 11.6 and 10.1, respectively. The similar modal Q's imply that both the in-phase and anti-phase modes contribute equally to radiation. Fig. 4 shows that both modes have a monopole-like radiation pattern. Fig. 5 indicates that the sum of the mode 1 and mode 9 admittances approximates the full-wave driven admittance locus and confirms that modes 1 and 9 are the only significant modes in this geometry.

III. Uncoupled Resonators

Given the preceding, we recognize two distinct resonators within the full geometry: an inner cylindrical cavity whose vertical wall is comprised of the ring of vias at r_1 and an outer *annular* planar inverted-F antenna (PIFA) whose shorting wall is formed by the ring of vias at r_1. Both are shown in Fig. 6; CMA these geometries yields *uncoupled* resonant frequencies $f_{\text{cavity}} = 5.51$ GHz $\equiv f_2$ and $f_{\text{PIFA}} = 5.17$ GHz $\equiv f_1$ with Q of 64 and 8.8, respectively. The significantly lower Q of the annular PIFA implies that it provides the primary radiation mechanism whereas the cavity radiates comparatively little. Because of the azimuthal symmetry, the annular PIFA radiation pattern is monopole-like.

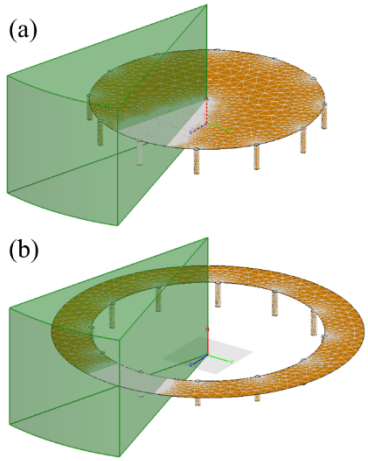

Fig. 6. Uncoupled resonator geometries: (a) cylindrical cavity and (b) annular PIFA. The infinite ground plane is not shown. The green wedge volumes show the volumes over which modal near-fields are calculated in order to calculate the coupling between the two resonators.

IV. Resonator Coupling & Coupled Mode Theory

The normalized coupling coefficient κ between the isolated resonators may be calculated via [9]:

$$\kappa = \kappa_e + \kappa_m = \frac{\int \epsilon E_1 \circ E_2 \, dV}{\sqrt{W_{e1} W_{e2}}} + \frac{\int \mu H_1 \circ H_2 \, dV}{\sqrt{W_{m1} W_{m2}}} \qquad (2)$$

where $W_{e1,2} = \int \epsilon |E_{1,2}|^2 dV$, $W_{m1,2} = \int \mu |H_{1,2}|^2 dV$ and $E_{1,2}$ and $H_{1,2}$ are the resonant modal near-fields of the uncoupled resonators. Due to the azimuthal symmetry present, resonant modal near-fields of each uncoupled resonator are calculated only within the wedge-volumes shown in Fig. 6 in cylindrical coordinates. The wedge volume extends 10 mm beyond r_2, is 5 h in height, and subtends an angle of $360°/12 = 30°$; there are (67, 17, 50) samples in the $(\hat{\rho},\hat{\phi},\hat{z})$ directions, respectively, or 56,950 total near field points. In addition, the mesh is refined within the wedge volume to produce high-quality data for field points near the conductors.

From (2), the nearfields give $\kappa_e = -0.108 - j0.033$ and $\kappa_m = 0.316 - j0.022$; the coupling is thus predominantly magnetic and $|\kappa| = 0.214$. Using $K \sim \kappa\omega_0/2$ [5], the coupled mode theory resonances of the combined structure are estimated using (1). These may be compared against the CMA-calculated coupled resonances $f_\pm$ of the Fig. 1 geometry. As in [7], a special geometry is used for calculating f_{cavity} to modestly improve the agreement between the CMT estimate and CMA results. The special geometry is equivalent to increasing the annular PIFA radius to infinity (similar to what was done in [5]). The is justified in that when the cavity resonator is combined with the annular PIFA, the capacitive parasitic at the cavity circular edge at $\rho = r_2 \cap z = h$ is reduced; this can be emulated—while eliminating the annular PIFA resonance—by increasing r_2 in Fig. 1 to infinity. The resonance calculated via this method is 5.73 GHz, about 4% higher than the resonant frequency of the Fig. 6(a) geometry.

The resulting CMT estimate for the in-phase coupled mode is $f_- = 4.80$ GHz and is nearly identical to the CMA-calculated value of 4.79 GHz. The CMT estimate for the anti-phase coupled mode is $f_+ = 6.11$ GHz, about 6% lower than the CMA-calculated value of 6.50 GHz.

V. Discussion & Comparison to Other Antennas

We now compare the modal behavior of the ACP geometry to that of other multi-modal patches also well-modeled by CMT: the U-slot patch [5], the E-shaped patch [6], stacked patches [7] and coplanar parasitically coupled patches [8]. Like [5] and [6], the in-phase and anti-phase modes of the ACP have similar, low Q's and similar radiation patterns, which provide a stable radiation pattern throughout the impedance bandwidth. Similar to [5] and [6], but unlike [8], in the ACP geometry one resonator (the cavity) radiates poorly and thus does not perturb the radiation pattern of the other resonator (the annular PIFA) when the currents are anti-phase at the upper range of the impedance bandwidth.

However, unlike [5] & [6] yet similar to [7] & [8], within the ACP impedance bandwidth the anti-phase mode (mode 9) impedance is predominantly reactive with much higher Q than the in-phase mode (mode 1). By 5.9 GHz, the admittance locus loop responsible for broad bandwidth has already significantly formed (see Fig. 5); below 5.9 GHz mode 9 is very reactive. Interestingly, the admittance of mode 1 begins to change trajectory around 5.2 GHz. At 5.9 GHz, both modes 1 and 9 suddenly change trajectory. This phenomenon is likely related to changes in modal current distributions associated with the eigenvalue crossing avoidance [4]. A similar phenomenon was observed in the stacked patch geometry [7], where the driven resonator (the lower patch) was interpreted to "double tune" [10] the primary radiating resonator (the upper patch). In this regard, the ACP is similar; we interpret the cylindrical cavity as a matching resonator and the annular PIFA as the radiating resonator.

VI. Conclusion

The annular coupled patch was analyzed with CMA; in-phase and anti-phase modes were shown to explain its broadband impedance. The geometry was decomposed into two resonators, a cavity and an annular PIFA. CMT was shown to model the coupled resonances of the combined geometry well. This insight can be used to develop a first-principles design methodology for the ACP and to suggest new antenna structures with desirable properties.

References

[1] J. Liu, Q. Xue, H. Wong, H. W. Lai and Y. Long, "Design and Analysis of a Low-Profile and Broadband Microstrip Monopolar Patch Antenna," in *IEEE Transactions on Antennas and Propagation*, vol. 61, no. 1, pp. 11-18, Jan. 2013.

[2] R. Harrington and J. Mautz, "Theory of characteristic modes for conducting bodies," in IEEE Transactions on Antennas and Propagation, vol. 19, no. 5, pp. 622-628, September 1971.

[3] S. L. Chuang, "Waveguide couplers and coupled mode theory" in Physics of optoelectronic devices, 1st ed., New York, NY, USA: Wiley, 1995, ch. 8, sec. 2.2, p. 291.

[4] K. R. Schab, J. M. Outwater, M. W. Young and J. T. Bernhard, "Eigenvalue Crossing Avoidance in Characteristic Modes," in IEEE Transactions on Antennas and Propagation, vol. 64, no. 7, pp. 2617-2627, July 2016.

[5] J. J. Borchardt and T. C. Lapointe, "U-Slot Patch Antenna Principle and Design Methodology Using Characteristic Mode Analysis and Coupled Mode Theory," in IEEE Access, vol. 7, pp. 109375-109385, 2019.

[6] J. Borchardt, "Analysis of an E-shaped Patch Using CMA and CMT," 2020 IEEE International Symposium on Antennas and Propagation and North American Radio Science Meeting, July 5-10, 2020 Montreal, Canada. To be published.

[7] J. Borchardt and T. LaPointe, "Analysis of a Stacked Patch Patch Using CMA and CMT," 2020 IEEE International Symposium on Antennas and Propagation and North American Radio Science Meeting, July 5-10, 2020 Montreal, Canada. To be published.

[8] J. Borchardt "Analysis of a Coplanar Parasitically Coupled Patch Antenna Using CMA and CMT," 2020 Asia-Pacific Micrwoave Conference, December 8-11, 2020, Hong Kong, SAR, China. To be published.

[9] J. Hong, "Couplings of asynchronously tuned coupled microwave resonators," in IEE Proceedings - Microwaves, Antennas and Propagation, vol. 147, no. 5, pp. 354-358, Oct. 2000

[10] A. R. Lopez, "Wheeler and Fano Impedance Matching [Antenna designer's notebook]," in IEEE Antennas and Propagation Magazine, vol. 49, no. 4, pp. 116-119, Aug. 200